Characterizing geothermal reservoirs using inverse methods

V. Rath *[v.rath@geophysik.rwth-aachen.de]*

1 Introduction

Inverse methods are a powerful tool when calibrating given computational models on observed data [3]. Most of the methods applied will produce estimates of error associated with the parameters determined as a by-product of the inversion technique. Unfortunately, forward simulators are much more developed than the corresponding inverse codes. We used *Automatic Differentiation* (AD) to derive the Jacobian codes from a given 3-D steady-state numerical solver for coupled flow and heat transport and its implementation within a Bayesian inverse model [8]. Currently, we are working on the implementation of time-dependent models, as well as the introduction of other physicochemical processes into the the inverse toolbox. Basic equations are given below.

$$\nabla \cdot \left(\frac{\rho_f g}{\mu_f} \mathbf{k} \cdot \nabla h \right) + Q = S \frac{\partial h}{\partial t} \tag{1}$$

$$\nabla \cdot (\lambda_e \nabla T) - (\rho c)_f \mathbf{v} \cdot \nabla T + A = (\rho c)_e \frac{\partial T}{\partial t} \tag{2}$$

$$\nabla \cdot (\sigma_e \nabla \phi) = -\nabla \cdot \mathbf{L} \left(\frac{\rho_f g}{\mu_f} \cdot \nabla h \right) \tag{3}$$

The red parts of the equations will be available in the near future. Currently, the following features are operational:

- quite general functions for fluid and rock properties, incorporated alt link time,
- nonlinear flow laws - useful for fracture flow,
- phase change (freezing/thawing),
- nonlinear solver based on fixed-point iteration or matrix-free Newton-Krylov,
- properties and boundary conditions realized by arbitrary zones,
- output in HDF5, VTK, Tecplot format.

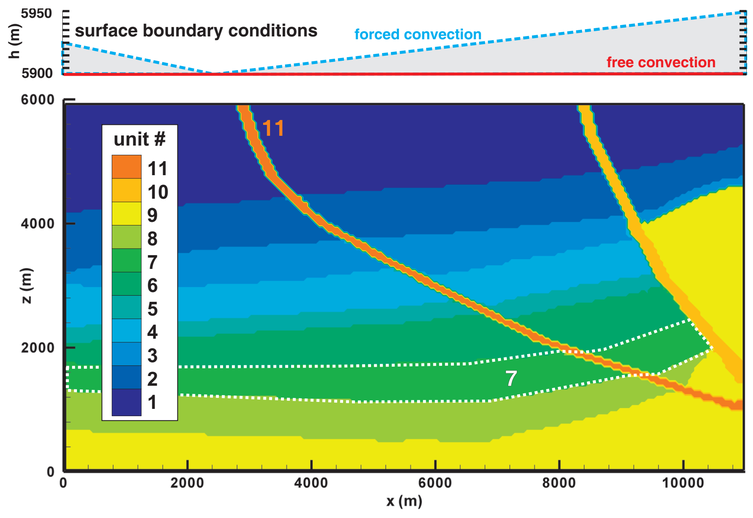

Figure 1: Model geometry for synthetic model. It is constructed from 11 units of different thermal and hydraulic properties. Units 1–8 represent sedimentary layers, while the salt diapir is associated with unit 9. The crosscutting faults which in this model are highly permeable, are units 10 and 11. Also shown is the assumed surface head driving the flow.

2 Inverse algorithm

A Bayesian inverse approach [13] is based on a model minimizing the nonlinear functional

$$\Theta_B = [\mathbf{d} - \mathbf{g}(\mathbf{p})]^T \mathbf{C}_d^{-1} [\mathbf{d} - \mathbf{g}(\mathbf{p})] + (\mathbf{p} - \mathbf{p}^a)^T \mathbf{C}_p^{-1} (\mathbf{p} - \mathbf{p}^a). \tag{4}$$

Here, $\mathbf{g}(\mathbf{p})$ refers to the forward model $\mathbf{d}$ is the observed data vector and $\mathbf{p}$ is the parameter vector. A priori values for parameters $\mathbf{p}^a$ and inverse covariance matrices $\mathbf{C}_d^{-1}$ and $\mathbf{C}_p^{-1}$ have to be known beforehand. A minimum can be found by a Gauss-Newton (GN) iteration

$$\mathbf{p}^{k+1} = \mathbf{p}^{k+i} + \mu \cdot \left(\mathbf{J}^T \mathbf{C}_d^{-1} \mathbf{J} + \mathbf{C}_p^{-1} \right)^{-1} \cdot \cdot \left\{ \mathbf{J}^T \mathbf{C}_d^{-1} \left[\mathbf{d} - \mathbf{g}(p^k) \right] - \mathbf{C}_p^{-1} \left[p^k - p^a \right] \right\} \tag{5}$$

or alternative formulations, where $\mathbf{J} = \partial \mathbf{g} / \partial \mathbf{p}$ refers to the Jacobian.

Our implementation includes:

- data: subsets of the nodal fields h and T calculated by the FD forward model, or linear combinations, i. e., point measurements, gradients or integrals of both data types,
- parameter: subsets or all of ϕ, a_x,a_y k_z, b_x,b_y,λ_z, and A for each zone, boundary zone properties,
- optional logarithmic parameter transformation,
- data and parameter space formulations of GN [13], and direct minimization of (4) by Nonlinear Conjugate Gradients (NLCG), or limited-memory Quasi-Newton techniques (e. g., LBFGS) [7],
- full or diagonal a priori covariances,
- optional calculation of covariances matrix a posteriori,

$$\mathbf{C}_p^{apo} = (\mathbf{S}^T \mathbf{C}_d^{-1} \mathbf{S} + \mathbf{C}_p^{-1})^{-1}, \tag{6}$$

and resolution matrices,

$$\mathbf{R}_d = \mathbf{I} - \left(\mathbf{J}^T \mathbf{C}_d^{-1} \mathbf{J} + \mathbf{C}_p^{-1} \right)^{-1} \mathbf{C}_p^{-1} = \mathbf{I} - \mathbf{C}_p^{apo} \mathbf{C}_p^{-1}. \tag{7}$$

3 Example: Bayesian inversion

To give an example, we calculated synthetic coupled 2-D models, schematically presenting the surroundings of salt diapir with cross-cutting tectonic faults. Model geometry (220×119) and the association of units is shown in Fig. 1. Unit 9 is associated with the nearly impermeable salt diapir, while units 10 and 11 represent the permeable fault zones. The model presented here is driven predominantly by density differences induced by a gradient of head imposed as a "topographic" boundary condition at the top ("forced convection"), though a contribution of varying temperature ("free convection") is also present. Considerable flow occurs orthogonal to the temperature isolines, i. e., $\mathbf{v} \cdot \nabla T \neq 0$ in large parts of the model.

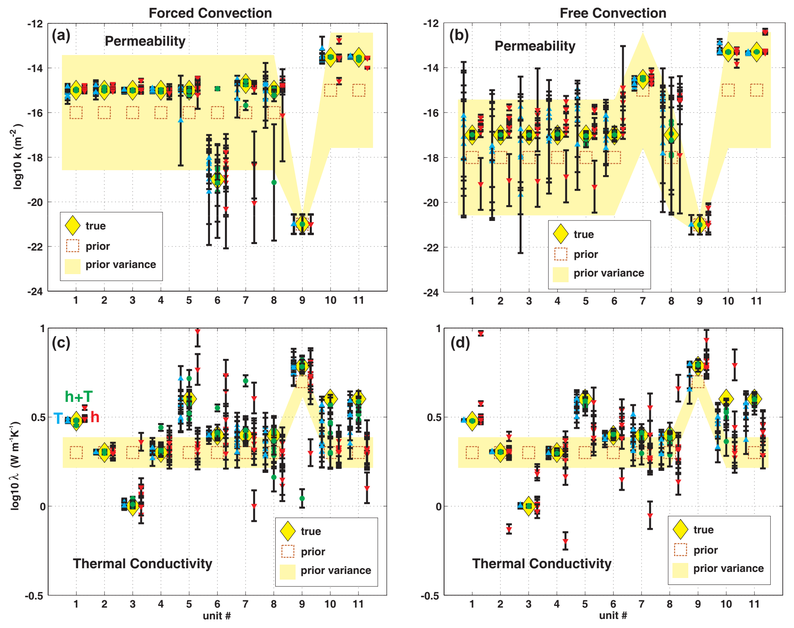

Figure 2: Inversion results for temperature data (blue upward triangles, shifted to the left), head data (red downward triangles, shifted to the right), and the combined data set (green circles, center). Error bars were calculated from Equation (6). (a) and (c) have been show the topographically driven case, while (b) and (d) come from the free convection example. Note that the parameters were taken as natural logarithms, implying that the assumed permeability errors of 6 correspond to a factor of more than two decades, while conductivities are usually believed to be more accurately known (≈ 20%). The priors were chosen with an non-trivial setup in mind

The setup described in Fig. 1. For each case, a set of 8 models was created. In each of these models, a given number of boreholes was generated, where site and depth were chosen at random. In particular, depth varied normally with a mean of 3500 m and a standard deviation of 1000 m. The data were subsequently modified, adding zero-mean normal noise with a standard deviation of 0.5 K for temperature, and 0.5 m for head, respectively. This choice of errors is disputable: though temperature can be continuously measured at high accuracy, technical and geological noise may easily reach this value. By geological noise we refer to small-scale parameter variations not accounted for in the model. The quasi-continuous head observations are somewhat idealized, because formation pressure is difficult to obtain in deep boreholes as assumed here. Often only integral values for special intervals or other derived quantities (e. g., Darcy velocities) are known. These conditions could be considerably different in a shallower regime, where temperature differences may be much smaller, and heads are much easier to determine with high accuracy.

The numerical experiment demonstrates the role of different data types. Temperature, head, and joined data sets were generated as described above. As expected, the determination of thermal conductivities requires temperature measurements. However, in cases with significant flow, the use of hydraulic data will reduce uncertainties, as advective effects may inhibit the estimation of conductive properties.

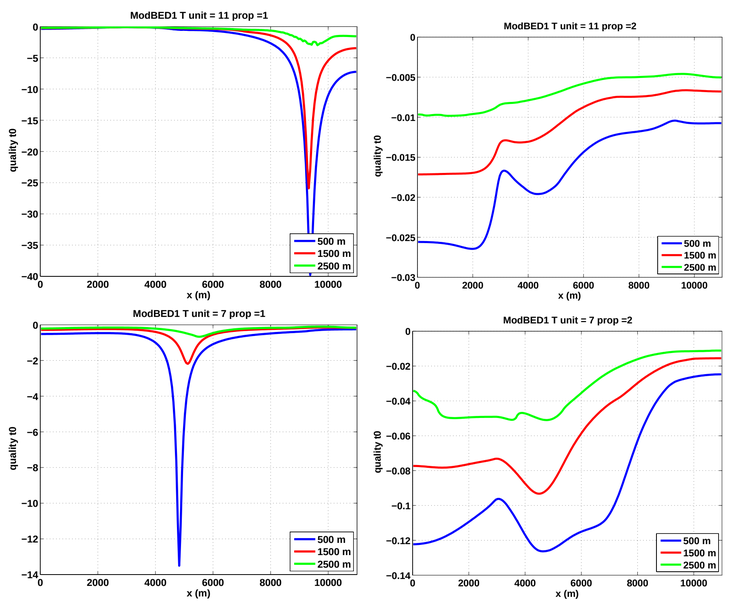

Figure 3: Design quality estimators t_0 for units 11 and 7 at the surface of the model shown in Fig. 1. Borehole depths of 500, 1500, and 2500 m are assumed.

4 Example: experimental design

Optimizing necessary or additional measurements, and judging their relevance for model generation is an important application of inverse theory. Starting from the Fisher Information Matrix $\mathbf{F} = \mathbf{J}^T \mathbf{C}_p^{-1} \mathbf{J}$, several common design quality indicators may be derived [1, 2], e. g.,

$$t_0 = -\sum_{i=1}^{N} \frac{1}{\lambda_i + \delta} \qquad t_3 = \sum_{i=1}^{N} \lambda_i = trace(\mathbf{F}). \tag{8}$$

5 Example: self-potential

Hydraulic data (formation pressures) are not easily accessible with in deep reservoirs. Therefore we suggest the use of self-potential (SP) observations to act as additional constraints of the model, as they can be obtained relatively cheaply at the surface, in non-cased boreholes, and even at the ocean bottom.

SP anomalies are caused by fluid flow through heterogeneous reservoirs. The sources of electrical potential are related to the hydraulic potential by the coupling coefficient

$$L = \frac{\epsilon \epsilon_0 \zeta}{\mu(\sigma + 2\sigma_s / r)} \rho g. \tag{9}$$

This means that SP is sensitive to spatial changes in the physical parameters in L, as well as to permeability. Most parameters in L are dependent on temperature, salinity, and other physicochemical (e. g., redox-potential). These relations are not well-known and represent an area of extensive research [11, 12, 9, 10, 4, 5, 6]. The proposed variations of L, however, are much smaller than the variations in permeability. Thus we believe, that even with these uncertainties, the inclusion of SP observation into the inverse scheme could lead to improved models. The fact that electrokinetic potentials are also coupled to temperature makes them particularly interesting when exploring geothermal reservoirs.

In Fig. 4show two models (calculated with COMSOL) as reference model and data source for our on SP inversion. They represent a very simple steady-state pumping scenario, in particular the role of the highly-conducting steel casing.

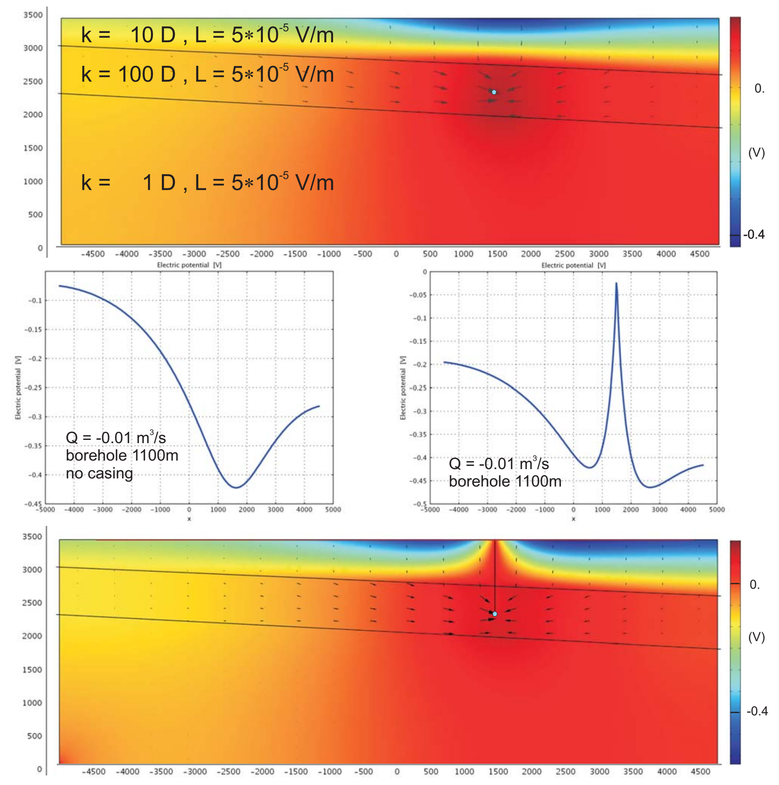

Figure 4: Design quality estimators t_0 for units 11 and 7 at the surface of the model shown in Fig. 1. Borehole depths of 500, 1500, and 2500 m are assumed.

References

[1] A. Curtis. Theory of model-based geophysical survey and experimental design. part 1 – linear problems. *The Leading Edge*, 23:997–1004, 2004.

[2] A. Curtis. Theory of model-based geophysical survey and experimental design. part 2 – nonlinear problems. *The Leading Edge*, 23:1112–1117, 2004.

[3] M. C. Hill and C. R. Tiedeman. *Effective Model Calibration: With Analysis of Data, Sensitivities, Predictions, and Uncertainty*. Wiley, New York, 2006.

[4] A. Maineult. *Aplication de la méthode du potentiel spontané à l'hydrogéologie: expérimentation sur modèle réduit d'aquifèreé*. PhD thesis, 2004.

[5] A. Maineult, Y. Bernabé, and P. Ackerer. Detection of advected concentration and pH fronts from self-potential measurements. *Journal of Geophysical Research*, 110:B11205, 2005.

[6] A. Maineult, Y. Bernabé, and P. Ackerer. Detection of advected, reacting redox fronts from self-potential measurements. *Journal of Contaminant Hydrology*, 86:32–52, 2006.

[7] J. Nocedal and S. J. Wright. *Numerical Optimization*. Springer, New York, 1999.

[8] V. Rath, A. Wolf, and M. Bücker. Joint three-dimensional inversion of coupled groundwater flow and heat transfer based on automatic differentiation: sensitivity calculation, verification, and synthetic examples. *Geophys. J. Int.*, 167:453–466, 2006.

[9] P. M. Reppert and F. D. Morgan. Temperature-dependent streaming potentials: 1. theory. *Journal of Geophysical Research*, 108:2546, 2003.

[10] P. M. Reppert and F. D. Morgan. Temperature-dependent streaming potentials: 2. laboratory. *Journal of Geophysical Research*, 108:2547, 2003.

[11] A. Revil, P. A. Pezard, and P. W. J. Glover. Streaming potential in porous media: 1. theory of the zeta potential. *Journal of Geophysical Research*, 104:20021–20031, 1999.

[12] A. Revil, H. Schwaeger, L. M. Cathles III, and P. D. Manhardt. Streaming potential in porous media: 2. theory and application to geothermal systems. *Journal of Geophysical Research*, 104:20033–20048, 1999.

[13] A. Tarantola. *Inverse Problem Theory. Methods for model parameter estimation*. SIAM, Philadelpha, 2004.